Effect of Cathodic Potentials on the Hydrogen Embrittlement Susceptibility of 10Ni5CrMo Steel

Pengfei Yin[1,2,], Xiangyang Li[1], Wenping Lu[2], Yalin Chen[2], Zhaohui Yang[2], Bo Zhang[2], Yong Guo[2], Jifeng Ding[2], Rongkai Cao[3]*

[1] Central Iron and Steel Research Institute, Beijing 100081, China
[2] Qingdao NCS Testing and Protection Technology Co., Ltd, Qingdao 266071, China
[3] College of Electromechanical Engineering, Qingdao University of Science and Technology, Qingdao 266061
[*]E-mail: ypf1201@163.com

The effects of the cathodic polarization potential on the hydrogen embrittlement susceptibility of 10Ni5CrMo steel in seawater were studied using a slow strain rate tensile test (SSRT) combined with observation of the fracture morphology and electrochemical measurements, as well as the hydrogen permeation test. The results showed that the rate controlling step of the cathode reaction changed from the oxygen depolarization reaction to the hydrogen depolarization reaction with the increase in the cathodic polarization level. With the negative shift in the polarization potential, the sample's reduction of area (R/A) and elongation decreased, and the fracture surfaces of the specimens displayed a transition from ductile microvoid coalescence to cleavage; however, the strength of the 10Ni5CrMo steel did not change significantly. The hydrogen embrittlement coefficient reached a threshold of 25%, while the polarization potential was approximately -992 mv (vs. SCE). In conclusion, the limiting cathodic protection potential of 10Ni5CrMo steel in a seawater environment was -992 mv.

1. INTRODUCTION

High strength steel has played an increasingly important role in the exploitation and utilization of marine resources. To reduce the corrosion rate of high strength steel in seawater, cathodic protection has become a common and feasible protection method. Research has shown that the higher the strength of steel is, the greater its hydrogen embrittlement susceptibility is [1-3]. Therefore, it is prudent to select the protective potential of high-strength steel. If the protective potential is too negative, hydrogen embrittlement will easily occur [4-6], as there are no obvious signs before hydrogen induced cracking,

and it hydrogen embrittlement very destructive to the structure. Thus, the research on the hydrogen embrittlement susceptibility of high strength steel is important in reducing the risk of catastrophic structure failures.

Some researchers have studied the hydrogen embrittlement susceptibility of high strength steel under cathodic protection, and a good understanding of the cathodic potential of medium and low strength steel has been achieved [6-9]. Additionally, there are specific standards to guide the engineering practice [10-12]. However, there are few studies on the cathodic protection potential of high-strength steel in seawater. Practical high-strength steels in the United States have an upper limit of cathodic protection potential of 700 MPa at -0.95 V [13]. The research on the hydrogen embrittlement susceptibility of a 900 MPa high-strength steel conducted by C. Batt et al. revealed that the cathodic protection potential of the test steel in seawater should be controlled between -0.77 V and -0.79 V [14]. In addition, the United States, France, Japan, South Korea have also studied the hydrogen embrittlement susceptibility of some high-strength steels [15-23]. In China, the hydrogen embrittlement sensitivity of 16Mn, X70, X80, X100, E690, 907, 921 and other high strength steels under cathodic polarization has been studied, and the hydrogen embrittlement coefficient has not exceeded 25% under the most negative cathodic protection potential [24-35].

The hydrogen embrittlement susceptibility among different types of steel is quite different. 10Ni5CrMo steel is an important type of steel in offshore engineering. Currently, there are no public reports on the hydrogen embrittlement susceptibility of 10Ni5CrMo steel. In this paper, the effect of the cathodic polarization potential on the hydrogen embrittlement susceptibility of 10Ni5CrMo steel in seawater was studied by electrochemical measurements, hydrogen permeation tests and slow strain rate tensile tests combined with the observation of the fracture morphology. These results can provide theoretical support for the selection of the cathodic protection potential of 10Ni5CrMo steel in seawater.

2.EXPERIMENTAL

The experimental material was 10Ni5CrMo steel, and its yield strength was 800 MPa. The experimental medium was natural seawater from the sea area near Qingdao Wheat Island. The dissolved oxygen content was approximately 8.5 mg/L, and the experimental temperature was 20°C. The other reagents used in the experiment were analytically pure, and the solution was prepared by redistilled water.

2.1 Polarization curve test

An EG&G PAR Model 2273 potentiostat was used for the polarization curve measurements that were conducted using a conventional three-electrode system. The test cell consists of a working electrode (specimen), platinum sheet as counter electrode and saturated calomel electrode (SCE) as reference. The electrochemical specimen was a square 10 mm×10 mm×2 mm sheet. Samples were sealed in a polyvinyl chloride tube with resin, and the test surface was reserved. The samples were then successively wet-

polished with 400-grit, 600-grit, 800-grit, 1000-grit, 1200-grit, 1500-grit, and 2000-grit silicon carbide (SiC) papers and degreased with ethanol and acetone prior to the experiment. The specimens were immersed in sea water for about 1 hour in order to obtain a relatively stable open circuit potential (OCP). The potential sweep range was set from -0.6 V (vs. OCP) to 0.05 V (vs. OCP) at a sweep rate was 20 mV/min.

2.2 hydrogen permeation test

An improved double-sided electrolytic cell method was used to detect the hydrogen permeation current using the method by Devanathan and Stachurski [36, 37]. The cell on the left was the cathode, and the cell on the right was the anode. The specimen was placed between the two cells as the working electrode. A saturated calomel reference electrode (SCE) was used in the cathode cell, and a Hg/HgO/ 0.1 M KOH reference electrode was used in the anode cell. The cathode current was applied on the specimen surface of the cathode cell using a potentiostat, and the anode potential (150 mV vs. Hg/HgO) was applied on the specimen surface of the anode cell in the electrochemical workstation. The specimens were square sheets of 20 mm×20 mm with a thickness of 0.35 mm. Both surfaces of the specimens were successively wet-polished with a series of grit SiC paper and degreased with ethanol and acetone prior to the experiment. Before conducting the hydrogen permeation test, the oxidation side of the specimen was coated with nickel in a Watt solution (250 g/L $NiSO_4 \cdot 6H_2O$, 45 g/L $NiCl_2 \cdot 6H_2O$, 45 g/L $NiCl_2 \cdot 6H_2O$, 40 g/L H_3BO_3) with a current density of 5 mA/cm^2 for 5 minutes. The anodic cell contained 0.2 mol/L NaOH under a potential of 150 mV (vs Hg/HgO). Before the penetration test, the cells were purged with high-purity nitrogen gas (99.99%) to remove the dissolved oxygen from the solution. Once the background current was decreased to a value below 0.1 $\mu A/cm^2$, the test solution was transferred to the hydrogen-charging cell and various cathodic potentials (-800 mV, -900 mV, -1000 mV, and -1100 mV) were applied to the entry sides of the specimens. In the anode cell, the permeated hydrogen was rapidly oxidized to generate a current that was monitored and recorded using a 2273 electrochemical workstation.

2.3 slow strain rate tensile test

The tensile test specimens were rod-shaped and prepared according to the China national standard, GB/T228-2002. The dimensions of the specimens are shown in Figure 1. The specimens were wet-polished with 2000-grit SiC paper and degreased with absolute ethanol and acetone. The experiments were performed in glycerol and seawater. An homemade electrochemical cell was adapted for working in the slow strain rate tension machine. The specimen used as working electrode was mounted on test machine and sealed in electrochemical cell by sealing ring. Platinum sheet and SCE were used as counter electrode and reference electrode. The polarization potentials were -800 mv, -900 mv, -1000 mv, and -1100 mv, applied by a ZF-3 potentiostat. Before stretching test, the constant potential polarization was applied to the specimens for 24 hours to eliminate the effect of hydrogen diffusion rate under different potentials,. Reference tests were performed in seawater at corrosion potential (E_{corr}) without polarized. The slow-strain rate tensile test was conducted by the Letry slow-stretching tester,

and the tensile rate was 0.005 mm/min. The load, displacement, and breakage time were automatically recorded by the computer. At the end of the experiment, the percentage elongation after fracture and elongation on the cross section were measured and calculated immediately. The macroscopic and microscopic morphology of the fracture surface were observed using a camera and a scanning electron microscope.
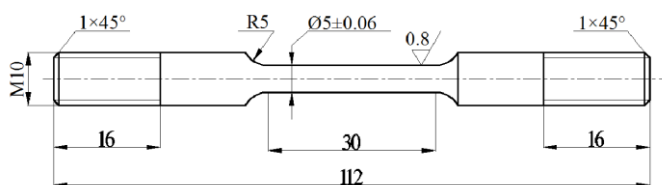
Figure 1. Specifications of the slow-strain-rate tensile test specimen.

3. RESULTS AND DISCUSSION

3.1 Potentiodynamic polarization curve

The potentiodynamic polarization curve of 10Ni5CrMo steel in seawater is shown as Figure 2. There were two turning points in the cathodic polarization curve. The first turning point is at approximately -650 mv, and the second turning point is at approximately -1000 mV. The corrosion potential (E_{corr}) was fitted to be -587 mV from the potentiodynamic polarization curve using the Tafel curve fitting method, which indicates that the cathodic reactions included an oxygen depolarization reaction and hydrogen depolarization reaction. The depolarization reactions of oxygen and hydrogen are shown in equation 1 and equation 2 [8, 10, 16], respectively. The rate controlling step of the cathode reaction before the first turning point A was the oxygen depolarization reaction [8]. At this stage, the cathode reaction on the metal surface was mainly the reduction reaction of oxygen in equation 1. After the turning point A, the rate controlling step of the cathode reaction became the oxygen diffusion to the electrode surface. The second turning point B indicates that the rate controlling step of the cathode reaction was converted from oxygen diffusion to the hydrogen depolarization reaction. After point B, with the negative shift in the electrode potential, the current density of the cathode increased rapidly, and the hydrogen evolution reaction of the cathode intensified. The cathode reaction was mainly a hydrogen evolution reaction, as shown in equation 2. Hydrogen evolution began to occur on the specimen surface, and the potential turning point 2 was usually called hydrogen evolution potential. The hydrogen evolution potential of the material was generally regarded as the most negative potential allowed for cathodic protection. If the protective potential is less than this value, the material may be in danger of hydrogen embrittlement. However, many studies showed that it is not reliable to regard the hydrogen evolution potential as the highest potential of cathodic protection [11, 16] because the cathode reaction is a comprehensive result of the reduction reactions of oxygen and hydrogen. Therefore, when the cathode polarization reaches a certain value, it will be accompanied by the reduction reaction of hydrogen. Only when the cathode polarization reaches a certain potential can the hydrogen escape the

metal surface. Before this potential, hydrogen generated by a hydrogen reduction reaction enters the metal, which will have a certain impact on the material performance. The hydrogen embrittlement susceptibility at various potentials should be verified by SSRT tests [16].
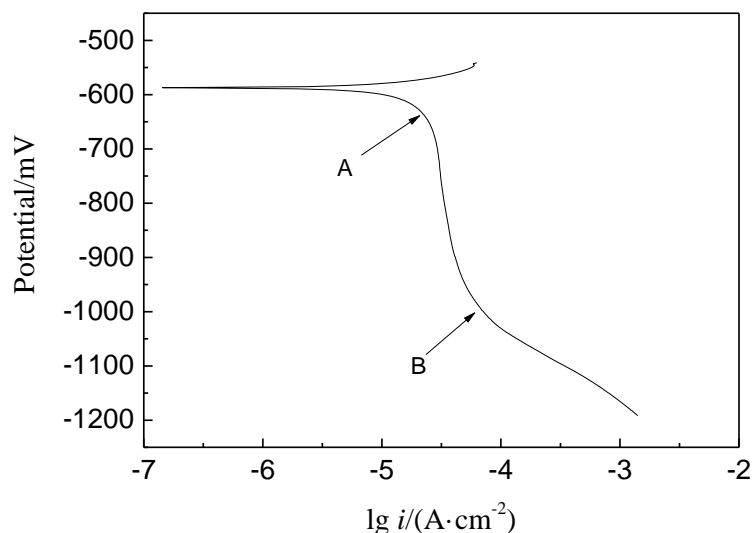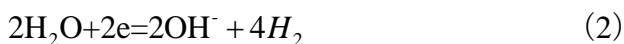
$$O_2 + 2H_2O + 4e = 4OH^- \qquad (1)$$

$$2H_2O + 2e = 2OH^- + 4H_2 \qquad (2)$$

Figure 2. Polarization curve of 10Ni5CrMo steel in seawater with a sweep rate of 20 mV/min.

3.2 Hydrogen permeation behavior

Figure 3 shows the hydrogen permeation current density curves of 10Ni5CrMo steel with different applied potentials. As shown in Figure 3, under different cathodic protection potentials, the hydrogen permeation current density increased rapidly with time and eventually became relatively stable. Capelle indicated that this phenomenon is related to the formation of calcium and magnesium deposits on the sample surface [28, 41]. The steady hydrogen permeation current density (i_H) varied greatly at various cathodic protection potentials; the more negative the potential is, the greater the i_H is.
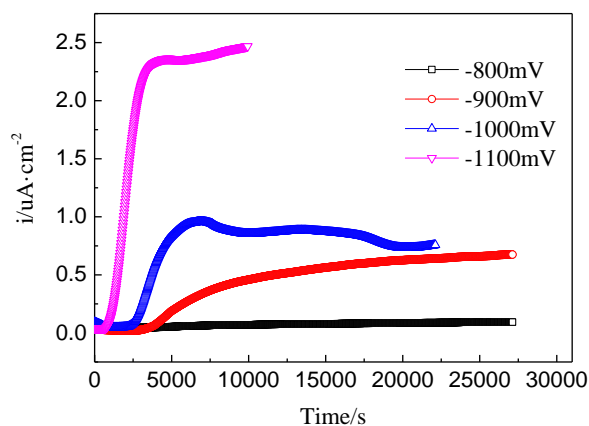

Figure 3. Hydrogen permeation current density curves of 10Ni5CrMo steel with different applied potentials (SCE) in seawater

When the polarization potential was -800 mV, the i_H was approximately 6×10^{-8} A/cm^2, and there was no hydrogen permeation. The i_H then increased significantly when the polarization potential was -900 mV, which was approximately 6.75×10^{-7} A/cm^2. i_H was approximately 8.2×10^{-7} A/cm^2 when the polarization potential was -1000 mV, and the surface of the material began to generate bubbles. When the potential reached -1100 mV, the i_H reached approximately 2.46×10^{-6} A/cm^2, which was 41 times greater than when the potential was -800 mV. A large number of bubbles appeared on the surface of the material. On the other hand, the greater the negative shift of the cathodic protection potential was, the shorter the time for i_H to reach steady state was, which indicated that more hydrogen evolution on the surface of the material made it easier for hydrogen diffusion in the material. By combining the potentiodynamic polarization curves, the negative shift of the cathodic polarization potential was observed, the cathodic reaction gradually moved from the oxygen depolarization reaction to the hydrogen evolution reaction, and the more negative the cathodic polarization potential was, the more pronounced the hydrogen evolution reaction was, *i.e.,* the more hydrogen atoms that were generated on the surface of the material, the more serious the hydrogen permeation of material was.

The hydrogen permeation flux (J_∞), effective diffusion coefficient (D) and sub-surface hydrogen concentration (C_0) can be obtained through the current density curve of the hydrogen permeation. The relationship between the hydrogen permeation flux (J_∞), and the saturation current density (i_∞) is as follows [38]:

$$J_\infty = \frac{i_\infty}{F} \qquad (3)$$

F is the Faraday constant, F = 9.65×10^4 s•A/mol.

The effective diffusion coefficient (D) can be calculated by the lag time (t_L) [39]:

$$D = \frac{d^2}{6t_L} \qquad (4)$$

In the formula, d is the specimen thickness, cm, t_L is the time when $i/i_\infty = 0.63$, s.

The sub-surface hydrogen concentration (C_0) is calculated by the following formula:

$$C_0 = \frac{i_\infty \cdot d}{F \cdot D} \qquad (5)$$

The hydrogen permeation parameters with different applied potentials (SCE) are listed in table 1. The lag time gradually decreased with the negative shift of the polarization potential from 13456 s to 2311 s, indicating that the diffusion rate of hydrogen in the material gradually increased. The effective diffusion coefficient D increased with the negative shift of the polarization potential, gradually increasing from 1.52×10^{-12} m^2/s to 8.83×10^{-12} m^2/s, and the hydrogen embrittlement susceptibility of the 10Ni5CrMo steel gradually increased. The D value changed significantly when the polarization potential was -1100 mV, indicating that the hydrogen embrittlement sensitivity of 10Ni5CrMo steel could be greatly increased with a slight change in potential when the cathodic protection potential was between -1000 mV and -1100 mV. Therefore, this interval should be avoided when the cathodic protection potential of 10Ni5CrMo steel was set. As shown in table 1, the sub-surface hydrogen concentration C_0 also increased with the negative shift of polarization potential [2, 3], gradually increasing from 1.43 mol/m^3 to 10.01 mol/m^3. The larger the C_0 is, the greater the gradient of hydrogen concentration on the surface and inside the material is, and then the hydrogen diffused inside the material more easily,

increasing the hydrogen embrittlement susceptibility of steel. As previously reported [2], due to the combined effect of hydrogen evolution reaction and calcareous deposits, there would be an extreme C_0 when the polarization potential is between -1000 mV and -1100 mV.

Table 1. Hydrogen permeation parameters of 10Ni5CrMo steel with different applied potentials (SCE).

| Polarization potential E/mV	Lag time t_L/s	Hydrogen permeation flux J_∞,mol/ $(cm^2 \cdot s)$	Effective diffusion coefficient D, m^2/s	Sub-surface hydrogen concentration C_0,mol/m^3
-800	13456	6.22×10^{-13}	1.52×10^{-12}	
-900	5417	6.99×10^{-12}	3.77×10^{-12}	6.49
-1000	3845	8.5×10^{-12}	4.21×10^{-12}	7.06
-1100	2311	2.55×10^{-11}	8.83×10^{-12}	10.01

3.3 Slow strain rate tensile test

Figure 4 shows the SSRT curves of 10Ni5CrMo steel in seawater and in an inert medium, glycerol. The elongation after fracture of 10Ni5CrMo steel in seawater was lower than that in glycerol, indicating that 10Ni5CrMo steel showed stress corrosion sensitivity in seawater that was below the self-corrosion potential.
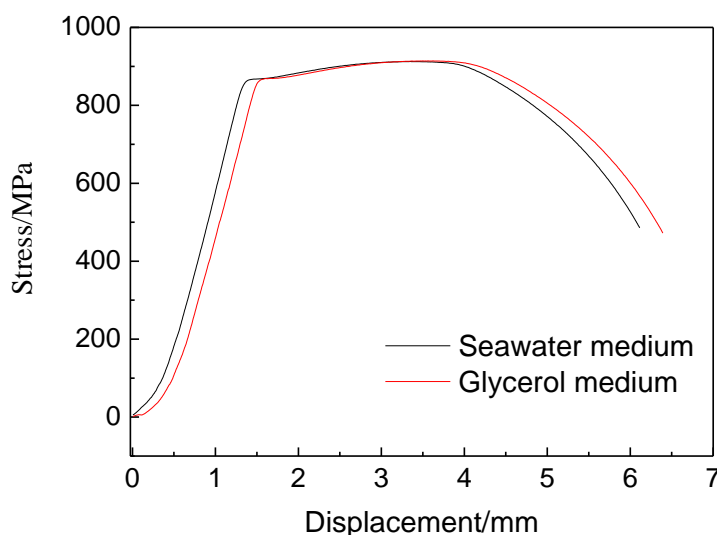
Figure 4. The SSRT curves of 10Ni5CrMo steel in seawater and glycerol.

According to the hydrogen permeability test results, the hydrogen concentration in the material increased with the negative shift of the cathode polarization potential. Studies have shown that under the

same conditions, the hydrogen concentration entering high-strength steel in the process of dynamic hydrogen charging and stretching is approximately 10 times that in the process of static hydrogen permeability [40], and the influence of diffusible hydrogen inside the high-strength steel on its mechanical properties is more obvious. The SSRT curves of 10Ni5CrMo steel with different polarization potentials in seawater are shown in Figure 5. The effect of the polarization potential on the mechanical properties of 10Ni5CrMo steel was not obvious prior to the stage of uniform plastic deformation. However, when the stress reached the material strength limit, the plastic deformation of the material showed a large difference. The more negative the polarization potential was, the smaller the plastic deformation of the material was, and the smaller the strain was. At the corrosion potential, the strain capacity of the material was 21.31%. After the cathode polarization was applied, the material strain capacity began to decrease. When the polarization potential was -800 mV, -900 mV, and -1000 mV, the strain capacity of the material was 19.58%, 19.01%, and 18.73%, respectively. When the polarization potential was -1100 mV, the plastic deformation of the material decreased greatly, and the strain capacity was 16.92%. Therefore, with the negative shift of the polarization potential, the ductility of the material decreased and the brittleness increased. The brittleness of the material significantly improved, especially when the potential reached -1100 mV.
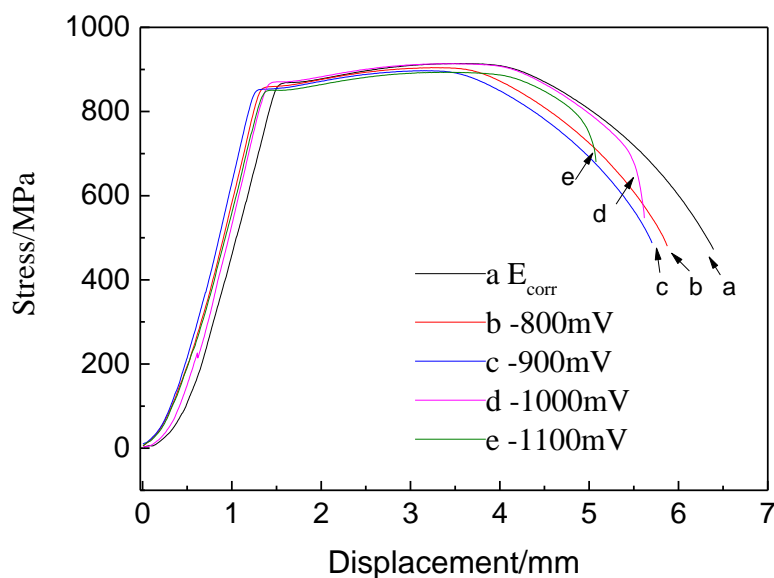
Figure 5. The SSRT curves of 10Ni5CrMo steel in seawater at E_{corr} and applied potential -800 mV, -900 mV, -1000 mV, -1100 mV(SCE)

Figure 6 shows some of the mechanical properties of 10Ni5CrMo steel under different conditions. The cathodic polarization potential had little effect on the yield strength and tensile strength of 10Ni5CrMo steel, which is consistent with the results of other scholars [2, 8, 16, 24, 26]. The yield strength (R_{eH}) of the material was between 848 MPa and 866 MPa, and the tensile strength (R_m) was between 893 MPa and 914 MPa. When the polarization potential was above -900 mV, the fracture strength (σ_f) of the materials changed little, staying at approximately 480 MPa, but when the value was

below -1000 mV, the fracture strength of the materials increased. The fracture strength at -1000 mV and -1100 mV was 547 MPa and 679 MPa, respectively, indicating that the brittleness of the material increased. Liu [2] concluded that a certain amount of hydrogen in the sample also played a role in improving the plasticity of the material. Overall, the cathode polarization had no effect on the strength index of 10Ni5CrMo steel.
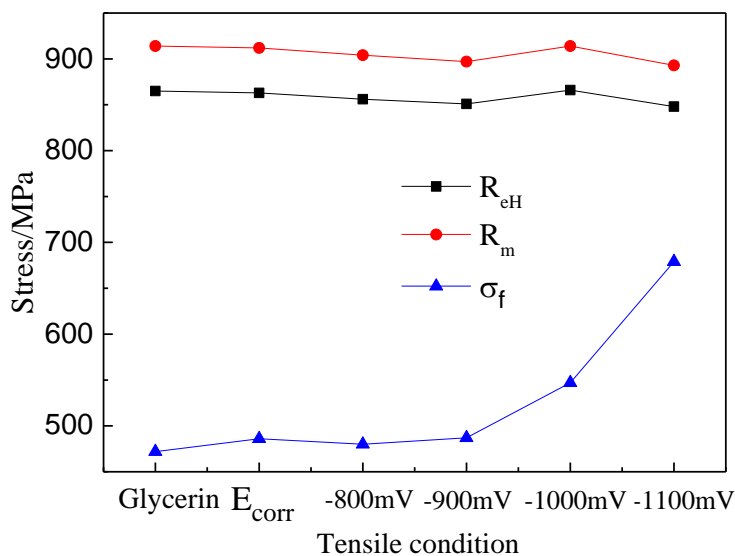
Figure 6. Strength properties of 10Ni5CrMo steel with different tensile conditions

Elongation and reduction of the cross-sectional area are widely recognized indicators for material plastic variation evaluation [18]. The 10Ni5CrMo steel-plastic indicators and change rule are shown in Figure 7 under different conditions. The elongation and reduction of the cross-sectional area for the specimen changed little when the polarization potential was between the self-corrosion potential and -900 mV, of which the elongation was 17.30–17.67% and the reduction of the cross-sectional area was 67.55–68.52%, which indicated that the plasticity of the material changed little. However, when the polarization potential was negative to -900 mV, the elongation and reduction of the cross-sectional area significantly decreased: the elongation was 17.60% at -900 mV, the elongation decreased to 14.27% at -1100 mV, and the percentage reduction of cross-sectional area decreased to 31.43% from 68.52%. When the polarization potential was negative to -900 mV, the material plasticity changed notably, and the hydrogen embrittlement susceptibility increased significantly. According to the electrochemical experiments, when the polarization potential was positive to -900 mV, the hydrogen evolution reaction was not obvious on the specimen surface, few hydrogen atoms entered the inner material from the specimen surface. In contrast, when the polarization potential was negative to -900 mV, the hydrogen evolution reaction was accelerated significantly and there were a large number of hydrogen atoms generated on the specimen surface. In addition, the hydrogen atoms inside the material increased, and the hydrogen embrittlement susceptibility of the material increased. It is noteworthy that although there existed a layer of calcium magnesium on the specimen surface at the polarization potential between -1000 mV and -1100 mV, the deposit did not prevent the hydrogen atoms from penetrating the material. Some scholars identified that [3] calcium and magnesium sediments generated on the surface of the

sample can reduce the penetration of hydrogen into a steel matrix to a certain extent. However, in the case of composite stress, the calcium and magnesium sediment on the sample surface can easily crack or even fall off, leading to an increase in the local polarization current density and an increase in the degree of hydrogen evolution, which improves the sensitivity of the material to hydrogen embrittlement.
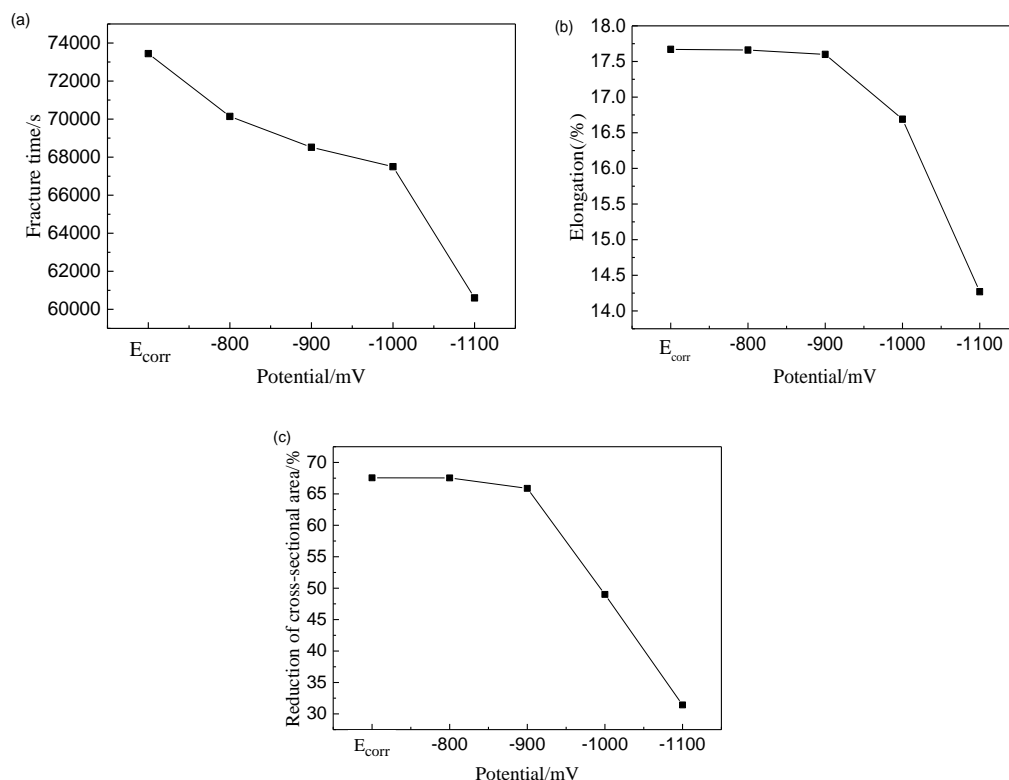

Figure 7. Fracture time(a), elongation(b), reduction of cross-sectional area(c) of 10Ni5CrMo steel at E_{corr} and applied potential -800 mV, -900 mV, -1000 mV, -1100 mV(SCE)

The coefficient of hydrogen embrittlement $F(\Psi)$ is generally utilized in engineering for quantitative evaluation of the hydrogen embrittlement susceptibility of materials [8, 17], as shown in Formula 6:

$$F(\Psi) = (\Psi_0 - \Psi)/\Psi_0 \times 100\% \qquad (6)$$

Where $F(\Psi)$ is the hydrogen embrittlement coefficient expressed by the reduction of cross-sectional area, Ψ_0 is the reduction of cross-sectional area of specimen in corrosive medium, and Ψ is the reduction of the cross-sectional area of the specimen in inert medium. Generally, $F(\Psi) < 25\%$ is deemed as a safe zone, $25\% \leq F(\Psi) \leq 35\%$ should be regarded as danger zone when hydrogen embrittlement is likely to occur. $F(\Psi) > 35\%$ is regarded as an embrittlement fracture zone in which hydrogen embrittlement fracture would occur. The $F(\Psi)$ results are shown in Figure 8. At the self-corrosion potentials, -800 mV and -900 mV, the $F(\Psi)$ of material was less than 5% and in the safe zone. When the polarization potential reached -1100 mV, $F(\Psi)$ increased to 54.36%, and the material entered the brittle failure zone. Based on the $F(\Psi)$ fitted curve, when the polarization potential was -983 mV, the $F(\Psi)$ was

25%. Therefore, the most negative protection potential of 10Ni5CrMo steel should not exceed -983 mV, otherwise hydrogen embrittlement fracture may occur.
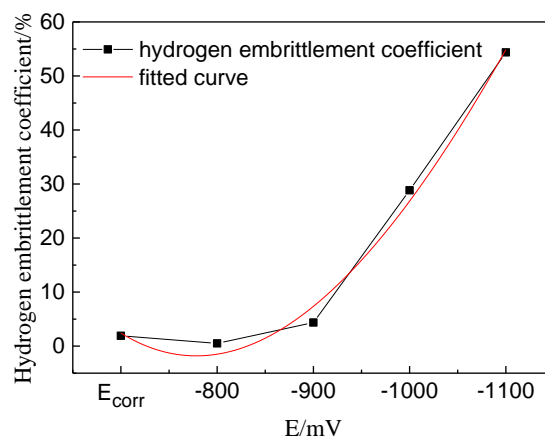

Figure 8. The Hydrogen embrittlement coefficient of 10Ni5CrMo steel at E_{corr} and applied potential -800 mV, -900 mV, -1000 mV, -1100 mV(SCE)

3.4 Fracture appearance analysis

The fracture appearance of tension specimen in glycerine and with various polarization potentials in seawater are shown in Figures 9 and 10. Under the action of glycerol and E_{corr}, the cup and cone-shaped fracture had obvious necking phenomenon, and the microscopic fracture had obvious dimples, which is typical of ductile fracture [16, 19], indicating that the specimen had no hydrogen embrittlement susceptibility at the time. With the negative shift of the polarization potential, the necking phenomenon of specimen fracture was not as obvious, the reduction of cross-sectional area gradually decreased, and the fracture mode changed from ductile to brittle fracture. When the polarization potential was -900 mV, the microscopic fracture morphology still had some dimples, indicating ductile fracture, and the hydrogen embrittlement susceptibility was not obvious. When the polarization potential was -1000 mV, the necking phenomenon of the fracture weakened obviously; a river-shaped pattern replaced the dimples. Furthermore, the fracture changed into a cleavage characteristic morphology, and the hydrogen embrittlement susceptibility increased greatly [2, 16, 35]. When the polarization potential reached up to -1100 mV, there was no necking phenomenon on the specimen fracture; in addition, a cleavage step, river-shaped pattern and other brittle fracture morphology appeared on the microscopic fracture, which indicated brittle fracture and hydrogen cracking [28].

In conclusion, with the negative shift in the polarization potential, the hydrogen content in the tensile sample increased, and the plastic loss of the material increased, gradually changing the fracture mode from ductile fracture to brittle fracture. This change was because in the process of slow stress stretching, dislocation migration occurs as the sample deforms and becomes the channel for hydrogen diffusion. At the same time, hydrogen atoms can promote dislocation emission, proliferation and movement, thus promoting local plastic deformation [42, 43, 44]. The accumulation of hydrogen atoms in the stress zone in the high-strength steel leads to the reduction of bonding force between the matrix

atoms. Moreover, with the negative shift of the cathode potential increasing, as more hydrogen atoms accumulate in the high-strength steel, the more serious the bond force decrease becomes. When the stress concentration caused by dislocation is equal to the hydrogen bonding force, microcracks begin to nucleate and expand in the sample [42, 45], causing a cleavage fracture. Elongation will gradually reduce the process of tensile stress and the reduction of area of the sample will be significantly lower, creating the hydrogen embrittlement phenomena. Therefore, the more negative the cathodic polarization potential is, the higher the hydrogen content in the material is, resulting in significantly more hydrogen embrittlement sensitivity. These results are consistent with other publications [2, 3, 6, 9,16,26].
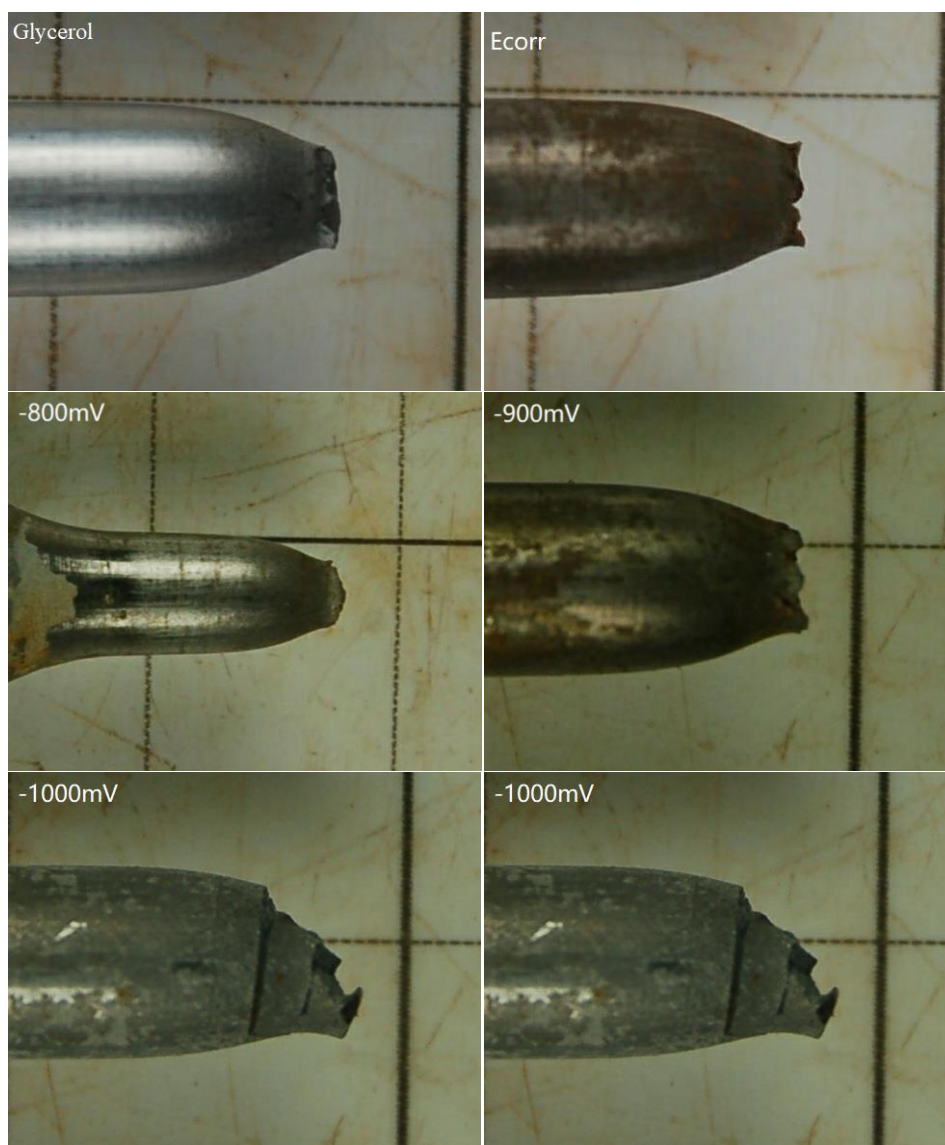
Figure 9. Macromorphology of the fracture surface of 10Ni5CrMo steel in glycerol and in seawater at E_{corr} and applied potential -800mV, -900mV, -1000mV, -1100mV(SCE)

(a) -800mV   (b) -900mV

(c) -1000mV   (d) -1100mV
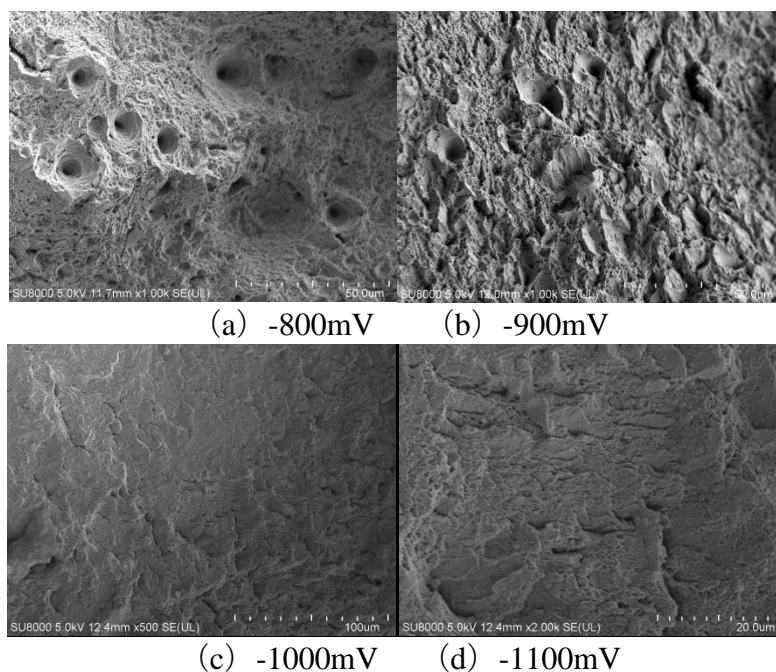
Figure 10. The fracture surface morphology of 10Ni5CrMo steel with different applied potentials(SCE)

4. CONCLUSION

（1）Electrochemical experiments of 10Ni5CrMo steel at different cathode polarization showed that with negative polarization potential, the cathode reaction first changed from activation control in oxygen depolarization reaction to diffusion control, and finally to the hydrogen depolarization reaction. The hydrogen evolution potential was approximately -1000 mV, and the more negative the cathode polarization potential was, the more serious the hydrogen evolution on the surface of the test material was.

（2）The cathodic polarization had significant impacts on the hydrogen permeation of 10Ni5CrMo steel in seawater. The steady hydrogen percolation current, effective diffusion coefficient, and apparent solubility increased with the negative shift in the cathodic polarized potential. When the cathodic protection potential was between -1000 mV and -1100 mV, the small potential variation greatly increased the hydrogen embrittlement susceptibility of 10Ni5CrMo steel.

（3）SSRT results indicates that the 10Ni5CrMo steel had no hydrogen embrittlement susceptibility in seawater at the self-corrosion potential. The plasticity of the 10Ni5CrMo steel decreased with the negative shift in the polarization potential, and the fracture mode changed to brittle fracture from ductile fracture. Within the E_{corr}~ -900 mV polarization potential, the $F(\Psi)$ of material was less than 5%, which was in the safe zone. When the polarization potential was -1000 mV, $F(\Psi)$ increased to 28.84%, and the material entered the danger zone. However, when the polarization potential was -1100 mV, $F(\Psi)$ increased to 54.36%, entering the brittle failure zone.

References

1. D. Shu, Mechanical properties of engineering materials, China machine press, (2007) Beijing, China.
2. Y. Liu, Y. li and Q. Li, *Acta. Metall. Sin*, 49 (2013) 1089.
3. T. Zhang, W. Zhao,W. Gu*, J. Chin. Soc. Corros. Prot.,* 34 (2014) 315.
4. D. Pan, X. Gao, L. Ma and Y. Yan, *Corros. Prot.*, 37 (2016) 225.
5. C. Lindley and W.J. Rudd, *Mar. Struct.*,14 (2001) 397.
6. D. Hardie, E.A. Charles and A.H. Lopez, *Corros. Sci.*, 48 (2006) 4378.
7. J. Billingham, J.V. Sharp, J. Spurrier and P.J. Kilgallon, Review of the Performance of High Strength Steels Used Offshore, *Health & Safety Executive*, (2003) Caerphilly, UK.
8. K. Qiu, B. Wei and Y. Fang, *J. Nanjing. Inst. Chem. Technol*, 14 (1992) 8.
9. X. Du, Y. Su, J. Li, L. Qiao and W. Chu, *Corros. Sci.*, 60 (2012) 69.
10. F. Zucchi, V. Grassi, C. Monticelli and G. Trabanelli, *Corros. Sci.*, 48 (2006) 522.
11. DNV-RP-F103, Recommended practice-cathodic protection of submarine pipelines by galvanic anodes. *Det Norske Veritas*, (2012), Norway.
12. NACE SP0169, Standard practice-control of external corrosion on underground submerged metallic piping systems. *NACE International*, (2007) Houston, USA.
13. J. N. Wankly, *Corros. Sci.*, 26 (1986) 66.
14. C. Batt, J. Dodson and M.J. Robinson, *Br. Corros. J.*, 37 (2002) 194.
15. I.L. Tazhibaeva and A.K. Klepiko, *Fusion. Eng. Des.*, 51 (2000) 199.
16. S.J. Kim, M. Okido and K.M. Moon, *Korean. J. Chem. Eng.*, 20 (2003) 560.
17. S. Komazaki, R. Maruyama and T. Misawa, *ISIJ. Int.*, 43 (2003) 475.
18. S.J. Kim, S.K. Jang, and J.I. Kim, *Met. Mater. Int.*, 11 (2005) 63.
19. T. Hara, Hydrogen embrittlement under cathodic protection for X100 and X120 high strength line pipes, *International Ocean and Polar Engineering Conference*, Hawaii, USA, 2015, 528.
20. L. Coudreuse, C. Renaudin, P. Bocquet and L. Cadiou, *Mar. Struct*, 10 (1996) 85.
21. A. Oni, *Constr. Build. Mater.*, 10 (1996) 481.
22. M. Wang, E. Akiyama and K. Tsuzaki, *Mat. Sci. Eng.* A, 398 (2005) 37.
23. I. Moro, L. Briottet, P. Lemoine, E. Andrieu, C. Blanc and G. Odemer, *Mat. Sci. Eng. A*, 527 (2010) 7252.
24. T.M. Zhang, W.M. Zhao, Y.J. Zhao, K.O. Yang, Q.S. Deng, Y.L. Wang and W. Jiang, *Int. J. Hydrogen Energy*, 43 (2018) 3353.
25. L. Zhang, W. Chao, K. Lu, Z. Wang, Y. Xing, Y. Du and M. Lu, *Int. J. Hydrogen Energy*, 42 (2017) 3389.
26. L. Zhang, H. Shen, J. Sun, Y. Sun, Y. Fang, W. Cao, Y. Xing and M. Lu, *Mater. Chem. Phys.*, 207 (2018) 123.
27. W. Zhao, T. Zhang, Y. Zhao, J. Sun and Y. Wang, *Corros. Sci.*, 111 (2016) 84.
28. T. Zhang, W. Zhao, T. Li, Y. Zhao and W. Jiang, *Corros. Sci.*, 131 (2018) 104.
29. H. Ma, Z. Liu, C. Du, X. Li and Z. Cui, *Mater. Sci. Eng. A*, 642 (2015) 22.
30. L. Zhang, H. Shen, K. Lu, W. Cao, Y. Sun, Y. Fang, Y. Xing, Y. Du and M. Lu, *Int. J. Hydrogen Energy*, 42 (2017) 29888.
31. H. Tian, X. Wang, Z. Cui, Q. Lu, L. Wang, L. Lei, Y. Li and D. Zhang, *Corros. Sci.*, 144 (2018) 145.
32. L. Zhang, M. Du and J. Liu, *Chin. J. Met. Sci. Technol.*, 19 (2011) 96.
33. X. Li, Y. Wang, P. Zhang, B. Li, X. Song and J. Chen, *Mat. Sci. Eng. A*, 616 (2014) 116.
34. E. Chang, Y. Yan, Q. li and L. Ma, *J. Chin. Soc. Corros. Prot.*, 30 (2010) 83.

35. K. Chang, J. Gu, H. Fang, Z. Yang, B. Bai and W. Zhang, *ISIJ. Int.*, 41 (2001) 1397.
36. M.J. Danielson, *Corros. Sci.*, 44 (2002) 829.
37. M.A.V. Devanathan, Z. Stachurski and W. Beck, *J. Electrochem. Soc.*, 10 (1963) 886.
38. S. Wang, W. Lu and K. Ho, *Mater. Chem. Phys.,* 77 (2002) 447.
39. X. Chen, X. Li, C.W. Du and P. Liang, *Acta. Metall. Sin.,* 44 (2008) 1431.
40. H.J. Maier, W. Popp and H. Kaesche. *Mat. Sci. Eng. A*, 191 (1995) 17.
41. J. Capelle, I. Dmytrakh and G. Pluvinage, *Corros. Sci.*, 52 (2010) 1554.
42. H. Li, W. Yang and K. Gao, *Acta. Metall. Sin*, 38 (2002) 849.
43. S. Sun, K. Shivzawa and J. Ga, *Metall. Trans.*, 26(1995) 731.
44. X. Wei, X. Zhou and W. Ke, *Acta. Metall. Sin.*, 29 (1993) 269.
45. J. Chen, W. Chu and Y. Wang, *Acta. Metall. Mater.*, 43(1995)4371.